EXPLICIT AND IMPLICIT TVD AND ENO HIGH RESOLUTION ALGORITHMS APPLIED TO THE EULER AND NAVIER-STOKES EQUATIONS IN THREE-DIMENSIONS – RESULTS

Edisson Sávio de Góes Maciel, edissonsavio@yahoo.com.br
Mechanical Engineer / Researcher – Rua Demócrito Cavalcanti, 152 – Afogados – Recife – PE – Brazil – 50750-080

Abstract. *In the present work, the Harten and Osher TVD/ENO and the Yee TVD symmetric schemes are implemented, on a finite volume context and using a structured spatial discretization, to solve the Euler and the laminar Navier-Stokes equations in the three-dimensional space. The Harten and Osher TVD/ENO schemes are flux difference splitting type, whereas the Yee TVD scheme is a symmetric one, which incorporates TVD properties due to the appropriated definition of a limited dissipation function. All three schemes are second order accurate in space. An implicit formulation is employed to all schemes in the solution of the Euler equations. The flux difference splitting schemes employ approximate factorizations in Linearized Nonconservative Implicit LNI form, whereas the symmetric scheme employs approximate factorization in ADI form. A spatially variable time step procedure is also implemented aiming to accelerate the convergence of the algorithms to the steady solution. The gains in convergence with this procedure were demonstrated in Maciel. The schemes are applied to the solution of the physical problems of the transonic flow along a convergent-divergent nozzle and of the supersonic flow along a compression corner in the inviscid case, whereas the laminar case studies a particular ramp problem. The results have demonstrated that the most accurate results are obtained with the Harten and Osher ENO and Yee TVD VL and Min1 schemes. This paper is the second part of this work, RESULTS, considering the presentation of the inviscid and laminar viscous results.*

Keywords*: Harten and Osher TVD/ENO algorithms, Yee TVD symmetric algorithm, Euler and Navier-Stokes equations, Laminar case, Explicit and implicit algorithms.*

1. INTRODUCTION

In the present work, the Harten and Osher (1987) TVD/ENO and the Yee (1987) TVD symmetric schemes are implemented, on a finite volume context and using a structured spatial discretization, to solve the Euler and the laminar Navier-Stokes equations in the three-dimensional space. The Harten and Osher (1987) TVD/ENO schemes are flux difference splitting type, whereas the Yee (1987) TVD scheme is a symmetric one, which incorporates TVD properties due to the appropriated definition of a limited dissipation function. All schemes are second order accurate in space and their numerical implementation is based on the concept of Harten's modified flux function. All three schemes are implemented following an implicit formulation to solve the Euler equations. The flux difference splitting schemes employ approximate factorizations in Linearized Nonconservative Implicit LNI form, whereas the symmetric scheme employs approximate factorization in ADI form. The viscous simulations are treated with the explicit versions of the present algorithms, which employ a time splitting method. The schemes are accelerated to the steady state solution using a spatially variable time step, which has demonstrated effective gains in terms of convergence rate (Maciel, 2005 and 2008). The algorithms are applied to the solution of the physical problems of the transonic flow along a convergent-divergent nozzle and of the supersonic flow along a compression corner in the inviscid case, whereas the laminar case studies a particular ramp problem. The results have demonstrated that the most accurate results are obtained with the Harten and Osher (1987) ENO and Yee (1987) TVD VL and Min1 schemes.

The main contribution of the present work to the CFD (Computational Fluid Dynamics) community is the extension of the Harten and Osher (1987) TVD/ENO schemes, as also the Yee (1987) TVD symmetric scheme, to three-dimensions, following a finite volume context, and their implicit implementation to inviscid problems, which characterizes a original contribution in the field of high resolution structured numerical algorithms.

The motivations to study the present numerical schemes and the implicit formulations, as well a review of the state of the art in the CFD community, are described in Maciel (2009), the first part of this work. This paper is the second part of this work, RESULTS, considering the presentation of the inviscid and laminar viscous results.

2. CONFIGURATIONS OF THE PHYSICAL PROBLEMS AND EMPLOYED MESHES

In this section, the physical configuration at the xy plane of the studied problems in this work is described altogether with the employed mesh in each case (inviscid and viscous laminar).

The geometry of the convergent-divergent nozzle at the xy plane is described in Fig. 1. The total length of the nozzle is 0.38ft (0.116m) and the throat height is equal to 0.090ft (0.027m). The throat is located at 0.19ft (0.058m) from the entrance boundary. The throat curvature ratio is equal to 0.090ft. The nozzle convergence angle is 22.33° and the nozzle divergence angle is 1.21°. An exponential stretching of 10% in both ξ and η directions was used. An algebraic mesh of 61 points in the ξ direction, 71 points in the η direction and 10 points in the ζ direction was generated, which

corresponds in finite volumes to 37,800 hexahedrons and 43,310 nodes. Its spanwise length is 0.10ft (0.0305m). Figure 2 exhibits the mesh employed in the simulations.

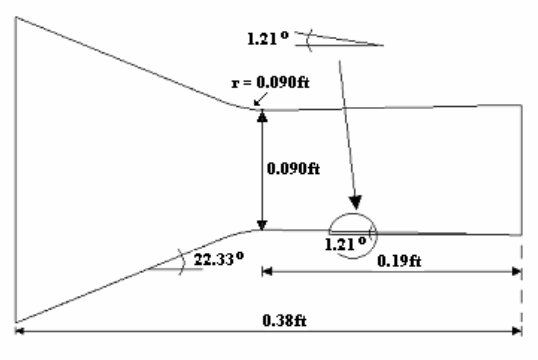

Figure 1. Nozzle configuration in the xy plane.

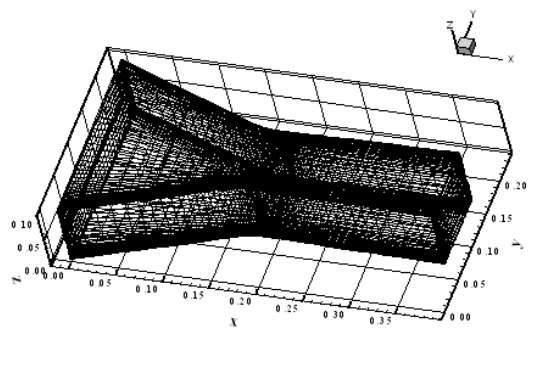

Figure 2. Nozzle mesh in three-dimensions.

The compression corner configuration at the xy plane is described in Fig. 3. The corner inclination angle is 10°. An algebraic mesh of 70 points in the ξ direction, 50 points in the η direction and 10 points in the ζ direction was generated, which corresponds in finite volumes to 30,429 hexahedrons and 35,000 nodes. Its spanwise length is 0.5m. Figure 4 exhibits such mesh.

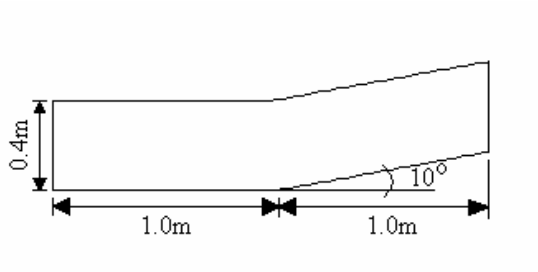

Figure 3. Corner configuration in the xy plane.

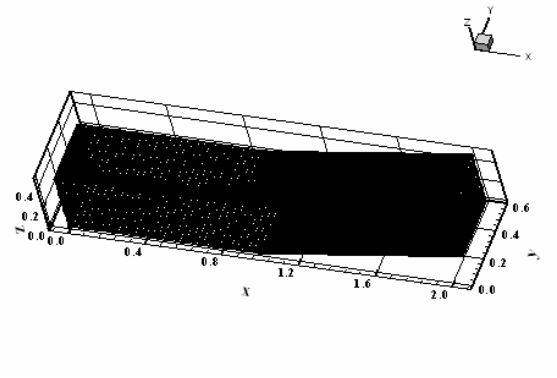

Figure 4. Corner mesh in three-dimensions.

Finally, the ramp configuration at the xy plane is described in Fig. 5. The compression corner has 20° of inclination. Its spanwise length is 0.25m. The mesh used in the simulations has 37,260 hexahedrons and 42,700 nodes to a structured discretization of the calculation domain. This mesh is equivalent, in finite differences, of being composed of 61 points in the ξ direction, 70 points in the η direction and 10 points in the ζ direction. An exponential stretching of 10% in the η direction was employed. Figure 6 shows such mesh. Table 1 presents a summary of the computational meshes.

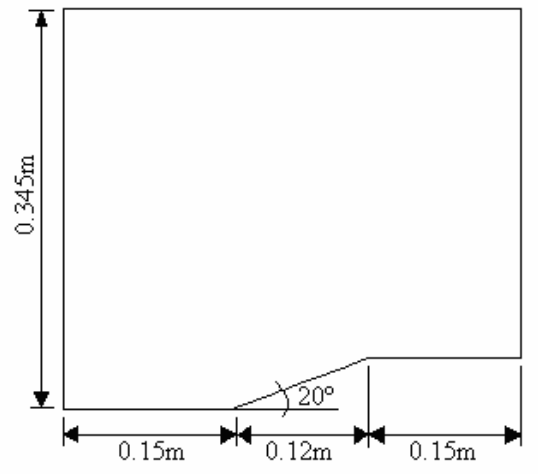

Figure 5. Ramp configuration in the xy plane.

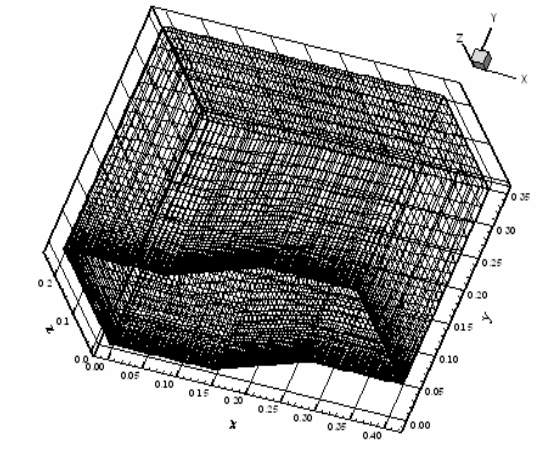

Figure 6. Ramp mesh in three-dimensions.

Table 1. Computational data of the meshes.

	Nozzle	Corner	Ramp
	61(ξ)x71(η)x10(ζ)	70(ξ)x50(η)x10(ζ)	61(ξ)x70(η)x10(ζ)
Cells	37,800	30,429	37,260
Nodes	43,310	35,000	42,700

3. RESULTS

Tests were performed in a microcomputer with processor AMD SEMPRON (tm) 2600+, 1.83GHz, and 512 Mbytes of RAM. As the interest of this work is steady state problems, one needs to define a criterion which guarantees that such condition was reached. The criterion adopted in this work was to consider a reduction of 3 orders in the magnitude of the maximum residual in the domain, a typical criterion in the CFD community. The residual to each cell was defined as the numerical value obtained from the discretized conservation equations. As there are five conservation equations to each cell, the maximum value obtained from these equations is defined as the residual of this cell. Thus, this residual is compared with the residual of the other cells, calculated of the same way, to define the maximum residual in the domain. The configuration upstream and the configuration longitudinal plane angles were set equal to 0.0°. All pressure distributions were determined at the plane corresponding to k = KMAX/2, where "KMAX" is the maximum number of points in the z direction, and j = 1, corresponding to the configuration wall.

To the inviscid cases, the implicit formulation was employed to generate the numerical results, whereas to the viscous laminar case, the explicit version of the numerical algorithms was used. It is important to remember from Maciel (2009) the nomenclature employed to the Yee's variants: Min1 (minmod1), Min2 (minmod2), Min3 (minmod3), SB (Superbee), and VL (Van Leer).

3.1. Inviscid results

3.1.1. Convergent-divergent nozzle

Stagnation flow was adopted as initial condition to this problem, with only a small reduction of the density and the pressure at the nozzle exit to initialize the flow.

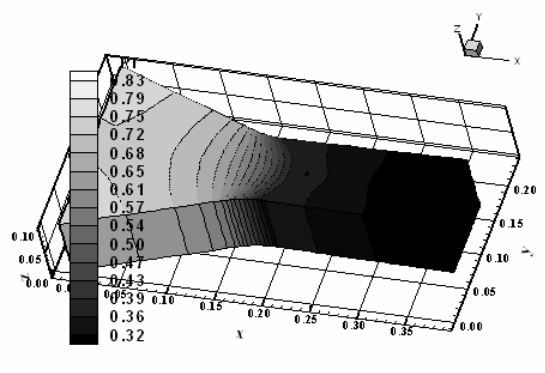

Figure 7. Pressure contours (HO-ENO).

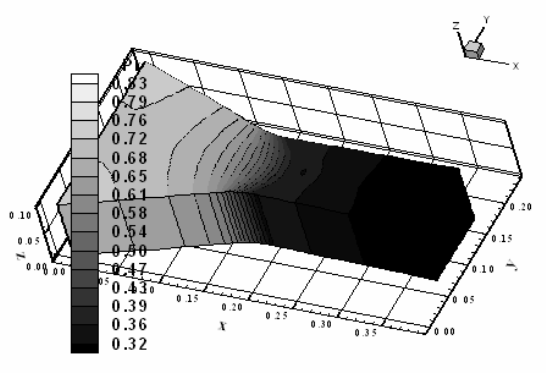

Figure 8. Pressure contours (HO-TVD).

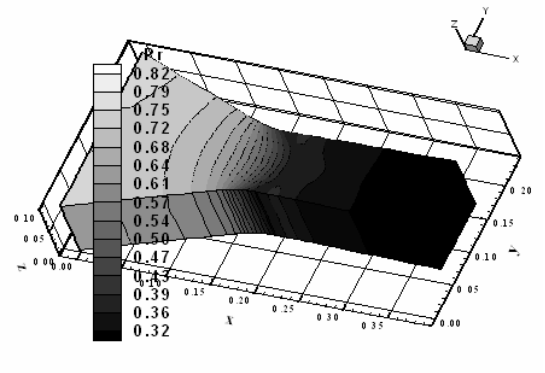

Figure 9. Pressure contours (Yee-Min1).

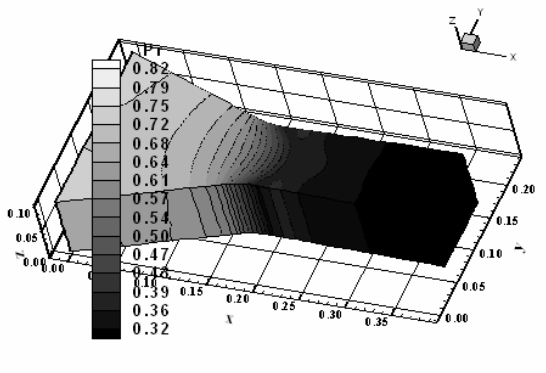

Figure 10. Pressure contours (Yee-Min2).

Figures 7 to 11 show the pressure contours obtained by the Harten and Osher (1987) ENO, Harten and Osher (1987) TVD, Yee (1987) Min1, Yee (1987) Min2 and Yee (1987) VL (Van Leer) schemes, respectively. The Yee (1987) Min3 and Yee (1987) SB (Superbee) schemes did not present converged results. The Harten and Osher (1987) TVD scheme presented the most severe pressure field in relation to the other schemes, representing a more conservative scheme to this problem. Good symmetry characteristics are observed in all solutions, with only some loss of quality in the solution generated by the Yee (1987) VL scheme.

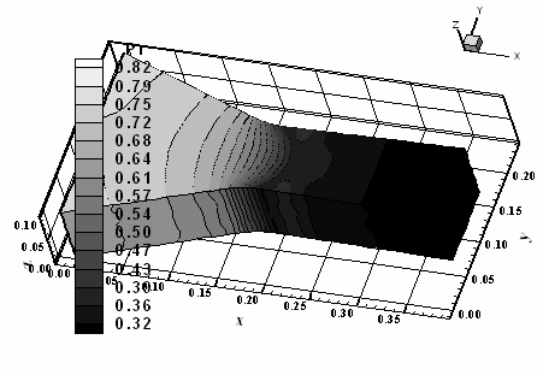

Figure 11. Pressure contours (Yee-VL).

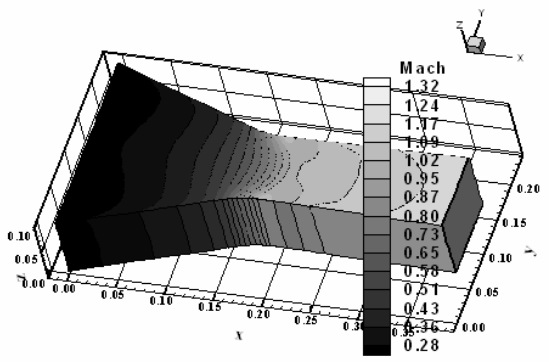

Figure 12. Mach number contours (HO-ENO).

Figures 12 to 16 present the Mach number contours obtained by the schemes of Harten and Osher (1987) ENO, of Harten and Osher (1987) TVD, of Yee (1987) Min1, of Yee (1987) Min2 and of Yee (1987) VL, respectively. The solution generated by the Harten and Osher (1987) TVD scheme is the most intense. All results present good symmetry properties, with only a small loss of symmetry in the solution generated by the Yee (1987) VL scheme.

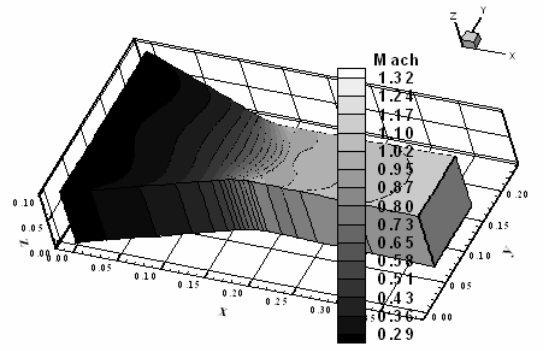

Figure 13. Mach number contours (HO-TVD).

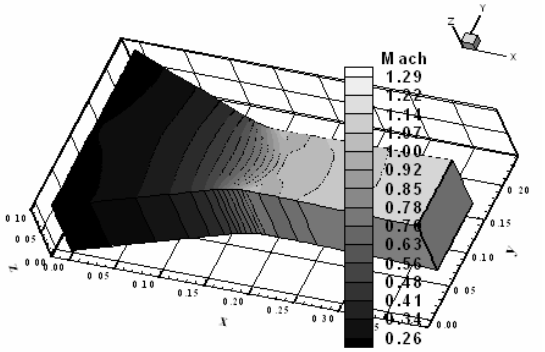

Figure 14. Mach number contours (Yee-Min1).

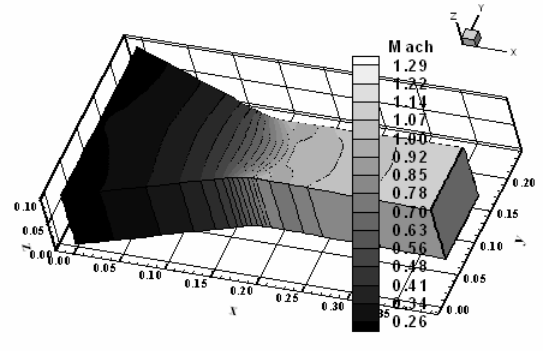

Figure 15. Mach number contours (Yee-Min2).

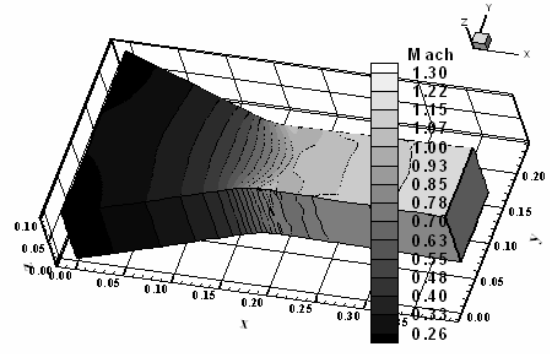

Figure 16. Mach number contours (Yee-VL).

Figure 17 exhibits the lower wall pressure distributions along the convergent-divergent nozzle. They are compared with the experimental results of Mason, Putnam and Re (1980). As can be observed, the Yee (1987) VL scheme presents the best pressure distribution (closer to the experimental results).

By this example, it was not possible to verify the attractive properties of the ENO schemes, which permits that the TVD conditions be relaxed, allowing the appearance of extremes in the solution, without generating oscillations. To the next example, a more severe aerodynamic problem, it is expected that the ENO properties be highlighted.

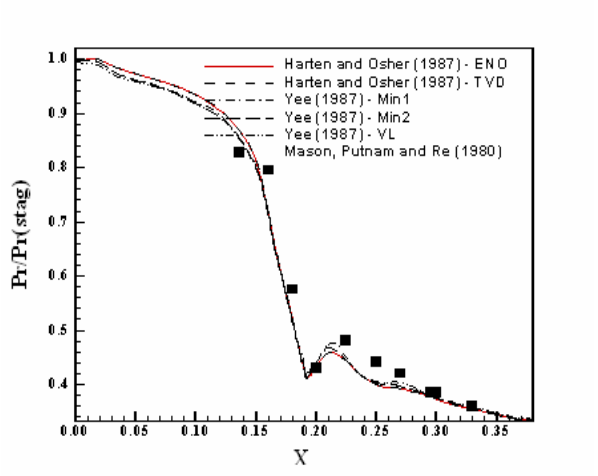

Figure 17. Wall pressure distributions.

3.1.2. Compression corner

A freestream Mach number of 3.0, characterizing a moderate supersonic flow regime, was adopted as initial condition to this problem. The flow reaches the compression corner, generating an oblique shock wave along the corner.

Figures 18 to 23 exhibit the pressure contours obtained by the schemes of Harten and Osher (1987) ENO, of Harten and Osher (1987) TVD, of Yee (1987) Min1, of Yee (1987) Min2, of Yee (1987) Min3 and of Yee (1987) VL, respectively. Only the Yee (1987) SB did not yield converged results. All solutions are clear, without pressure oscillations. The Yee (1987) Min3 scheme yields the most severe pressure field in relation to the other schemes, representing a more conservative scheme to this problem.

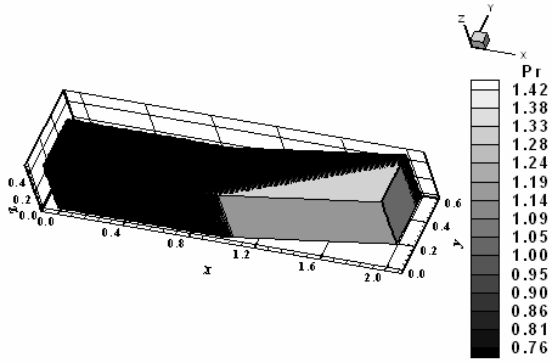

Figure 18. Pressure contours (HO-ENO).

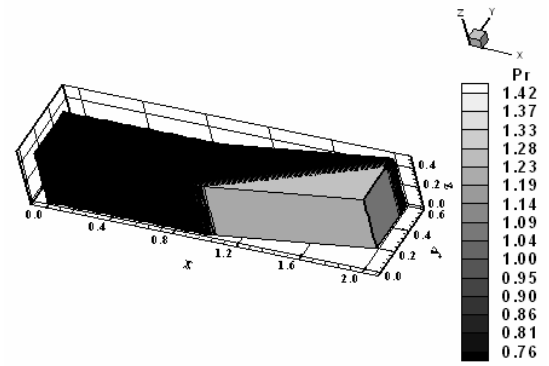

Figure 19. Pressure contours (HO-TVD).

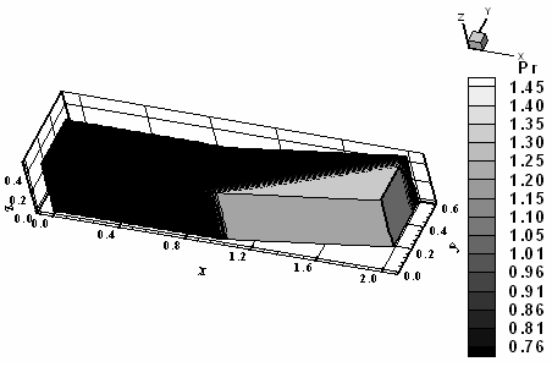

Figure 20. Pressure contours (Yee-Min1).

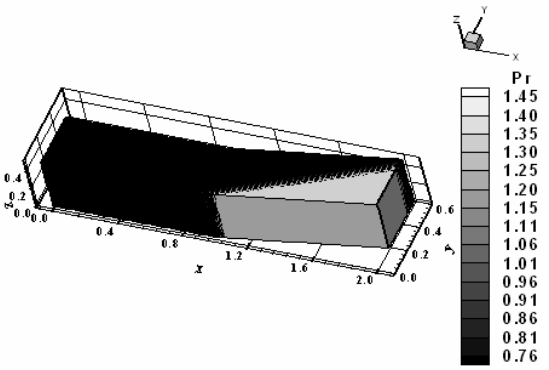

Figure 21. Pressure contours (Yee-Min2).

Figures 24 to 29 show the Mach number contours obtained by the Harten and Osher (1987) ENO, the Harten and Osher (1987) TVD, the Yee (1987) Min1, the Yee (1987) Min2, the Yee (1987) Min3 and the Yee (1987) VL schemes, respectively. The most intense Mach number field is obtained by the Yee (1987) VL algorithm. All solutions are clear and without oscillations.

Figure 30 exhibits the wall pressure distributions along the compression corner obtained by all schemes. They are compared with the oblique shock wave theory results.

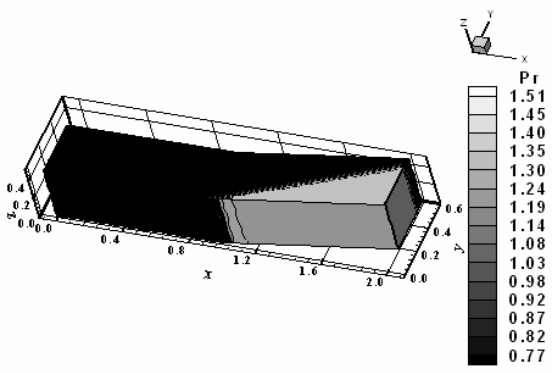

Figure 22. Pressure contours (Yee-Min3).

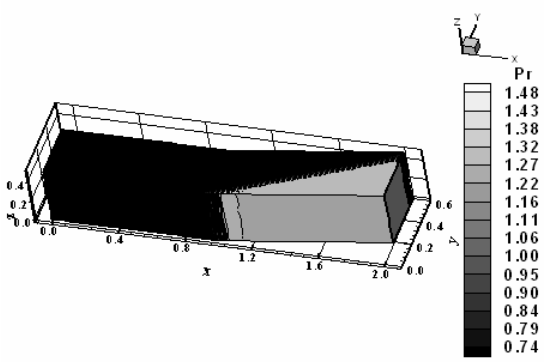

Figure 23. Pressure contours (Yee-VL).

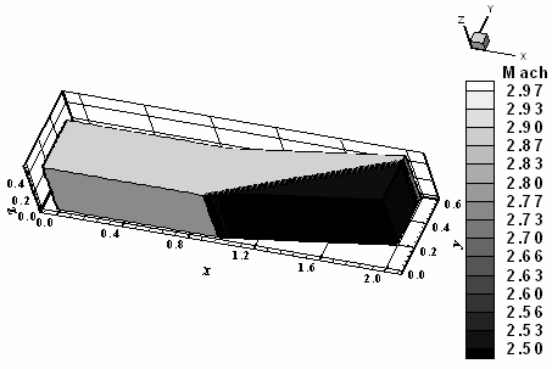

Figure 24. Mach number contours (HO-ENO).

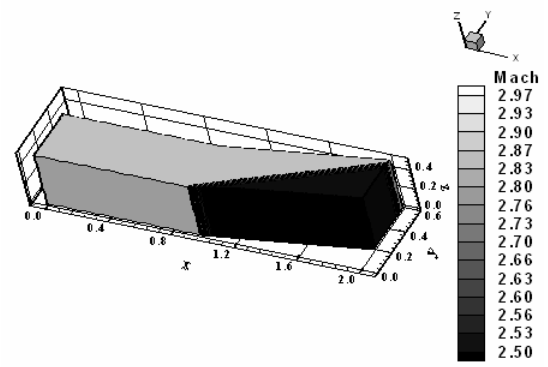

Figure 25. Mach number contours (HO-TVD).

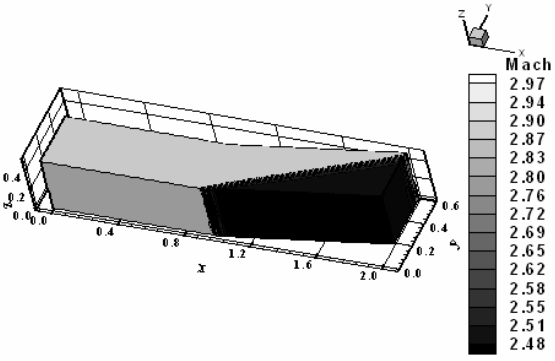

Figure 26. Mach number contours (Yee-Min1).

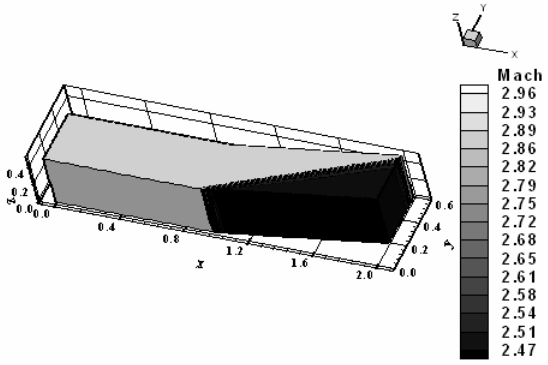

Figure 27. Mach number contours (Yee-Min2).

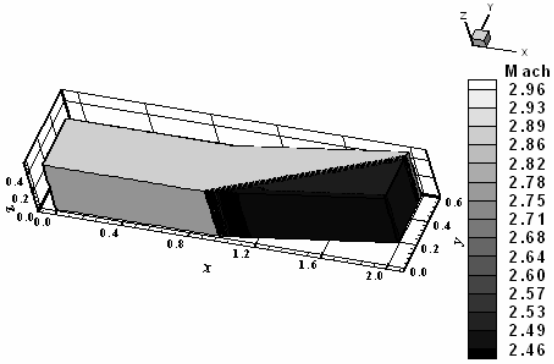

Figure 28. Mach number contours (Yee-Min3).

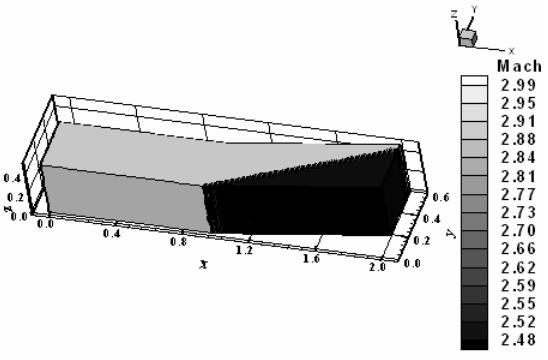

Figure 29. Mach number contours (Yee-VL).

As can be observed, the Harten and Osher (1987) ENO and TVD variants do not present oscillations at the discontinuity. The Yee (1987) TVD symmetric variants present some oscillations at the discontinuity. These features are more clearly demonstrated in Figs. 31 and 32. In Figure 31, only the Harten and Osher (1987) ENO and TVD variant results are shown. As can be highlighted, these solutions are free of oscillations near the discontinuity and both capture the shock wave in three cells, which is a good prediction in terms of shock capturing. In Figure 32, the solutions of the Yee (1987) TVD scheme in its variants are exhibited and, as previously mentioned, some oscillations occur at the

discontinuity. Even so, the shock wave is captured in three cells, which represents a good prediction of these schemes. As conclusion, in this example was possible to highlight the great improvement in shock capturing due to the concept of ENO (Essentially Non-oscillatory Schemes), which allowed the capture of the shock discontinuity without oscillations, only due to some relaxation in the TVD conditions (allows some extreme formations in the field without, however, generating oscillations), assuring uniformly second order accuracy in the computational domain.

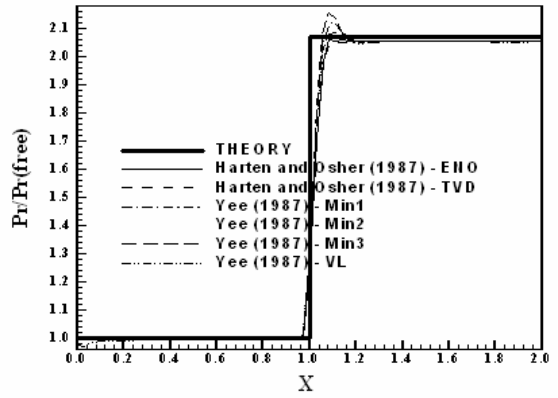

Figure 30. Wall pressure distributions.

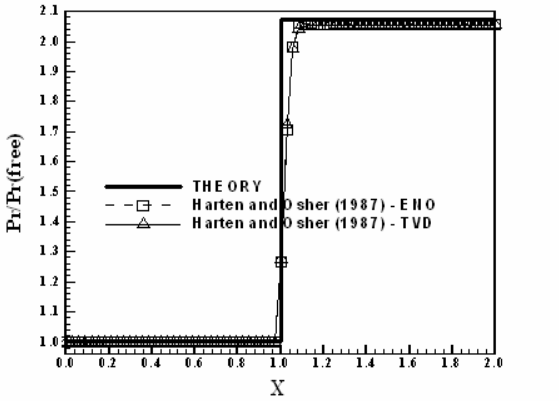

Figure 31. Wall pressure distributions (HO).

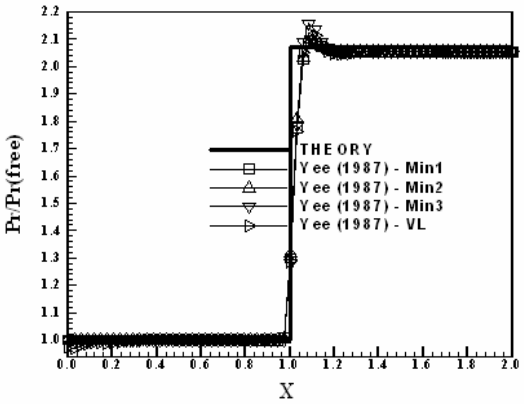

Figure 32. Wall pressure distributions (Yee).

One way to quantitatively verify if the solutions generated by each scheme are satisfactory consists in determining the shock angle of the oblique shock wave, β, measured in relation to the initial direction of the flow field. Anderson Jr. (1984) (pages 352 and 353) presents a diagram with values of the shock angle, β, to oblique shock waves. The value of this angle is determined as function of the freestream Mach number and of the deflection angle of the flow after the shock wave, ϕ. To the compression corner problem, $\phi = 10^{o}$ (ramp inclination angle) and the freestream Mach number is 3.0, resulting from this diagram a value to β equals to 27.5º. Using a transfer in Figures 18 to 23, considering the xy plane, it is possible to obtain the values of β to each scheme, as well the respective errors, shown in Tab. 2. As can be observed, the best schemes were the Harten and Osher (1987) ENO and the Yee (1987) TVD VL ones.

Table 2. Shock angle and respective percentage errors to the corner problem.

Algorithm	β(°)	Error (%)
Harten and Osher (1987) ENO	27.40	0.36
Harten and Osher (1987) TVD	27.75	0.91
Yee (1987) TVD Min1	27.00	1.82
Yee (1987) TVD Min2	27.00	1.82
Yee (1987) TVD Min3	27.00	1.82
Yee (1987) TVD VL	27.40	0.36

3.2. Viscous results

In the viscous studies only simulations with the Harten and Osher (1987) ENO and TVD versions and Yee (1987) Min1 and Min2 versions yielded converged results. The other limiters due to the Yee (1987) scheme did not produce steady state solutions.

The physical problem studied in the viscous laminar simulations is the flow along a ramp. This problem is a supersonic flow hitting a ramp with 20° of inclination. It generates a shock and an expansion fan. The freestream Mach number adopted as initial condition to this simulation was 2.0, characterizing a low supersonic flow. The Reynolds number was estimated to be 1.613×10^5 at a flight altitude of 20,000m and l = 0.0437m, based on the work of Fox and McDonald (1988).

Figures 33 to 36 exhibit the pressure contours obtained by the Harten and Osher (1987) ENO, Harten and Osher (1987) TVD, Yee (1987) Min1 and Yee (1987) Min2 schemes, respectively. The most severe pressure field, which characterizes the most conservative solution, is obtained by the Harten and Osher (1987) TVD scheme. It is possible to observe in all solutions the formation of a weaker shock ahead of the compression corner due to the increase of the boundary layer thickness. It suggests the formation of a separation region with development of a circulation bubble ahead of the ramp, where there is loss of pressure and energy.

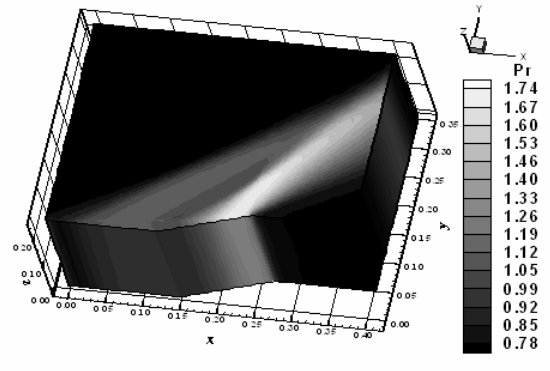

Figure 33. Pressure contours (HO-ENO).

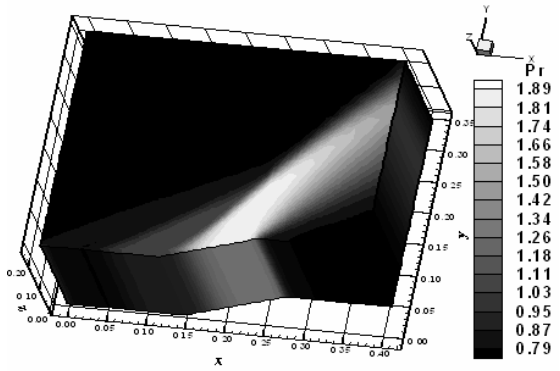

Figure 34. Pressure contours (HO-TVD).

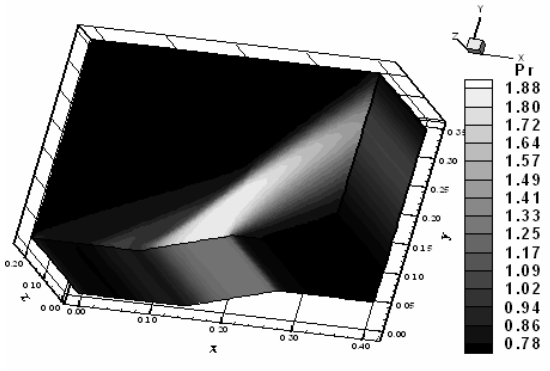

Figure 35. Pressure contours (Yee-Min1).

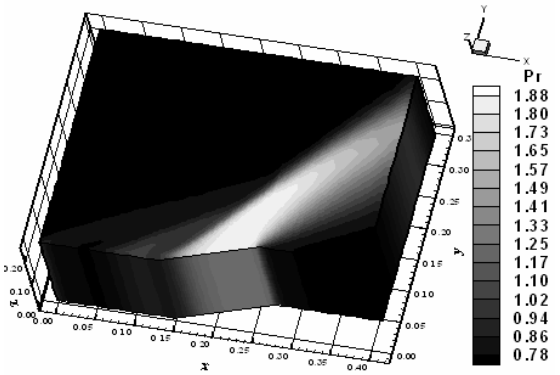

Figure 36. Pressure contours (Yee-Min2).

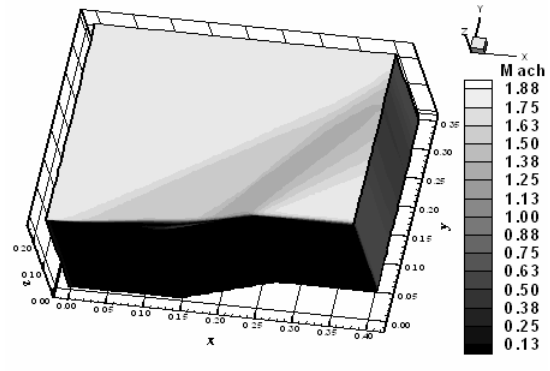

Figure 37. Mach number contours (HO-ENO).

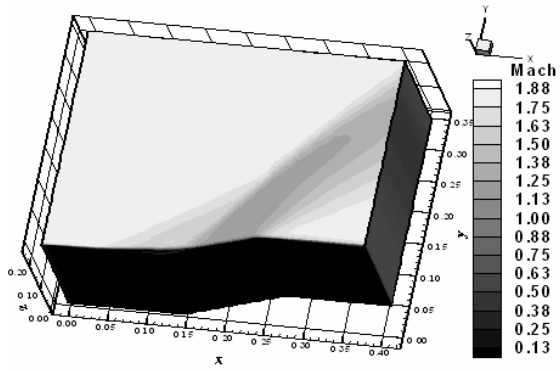

Figure 38. Mach number contours (HO-TVD).

Figures 37 to 40 show the Mach number contours obtained by the schemes of Harten and Osher (1987) ENO, of Harten and Osher (1987) TVD, of Yee (1987) Min1 and of Yee (1987) Min2, respectively. The Mach number contours generated by the Yee (1987) Min1 and Min2 variants are more intense fields than those generated by the Harten and Osher (1987) variants. Again, the appearance of a weaker shock before the ramp indicates the excessive raise of the

boundary layer thickness and the possible formation of a separation region with the development of a circulation bubble region.

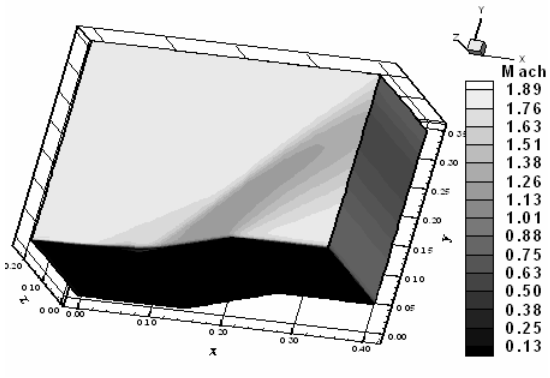

Figure 39. Mach number contours (Yee-Min1).

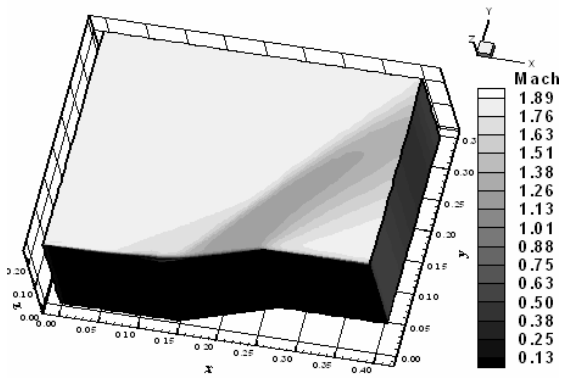

Figure 40. Mach number contours(Yee-Min2).

Figures 41 to 44 exhibit the velocity vector fields and the streamlines, at the xy plane, obtained by each scheme close to the ramp wall. It is possible to observe that all schemes detect the separation region with the formation of a circulation bubble. The biggest separation region is detected by the Harten and Osher (1987) ENO scheme, whereas the minimum region of separation is captured by the Yee (1987) symmetric Min2 scheme. Moreover, the Yee (1987) solutions presents more discrete flow separations, which is demonstrated in the solutions of pressure and Mach number contours, where even detecting the weaker shock, it is less severe than those of the Harten and Osher (1987) solutions. As conclusion, all four schemes detect the flow separation and the circulation bubble formation at the corner of the ramp, characterizing a region of physical instability, where occurs loss of pressure and energy.

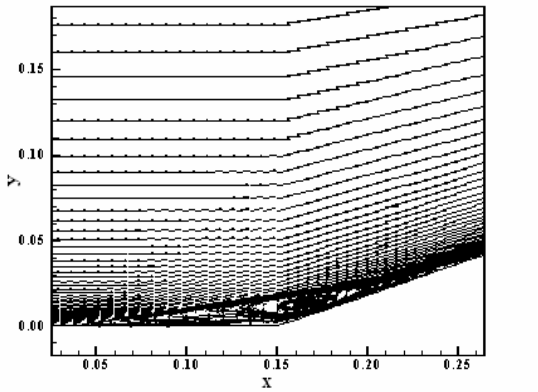

Figure 41. Velocity field and streamlines (HO-ENO).

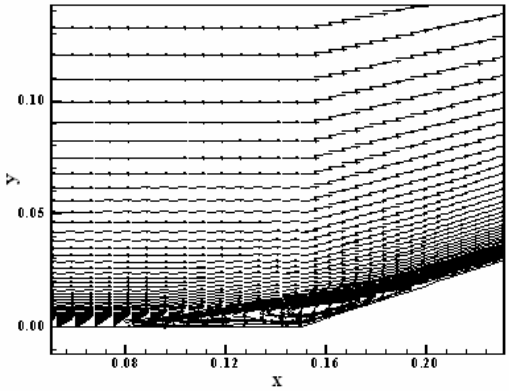

Figure 42. Velocity field and streamlines (HO-TVD).

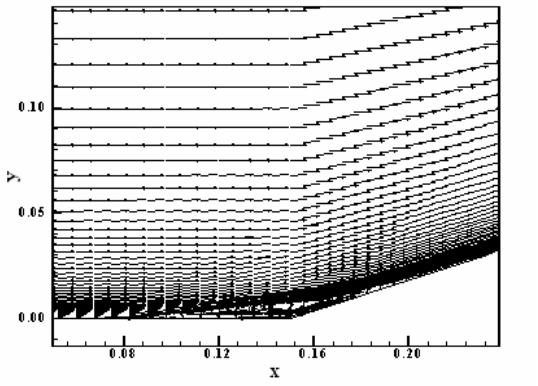

Figure 43. Velocity field and streamlines (Yee-Min1).

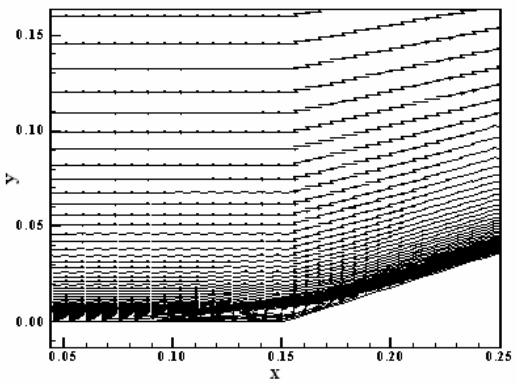

Figure 44. Velocity field and streamlines (Yee-Min2).

Again, one way to quantitatively verify if the solutions generated by each scheme are satisfactory consists in determining the shock angle of the oblique shock wave, β, measured in relation to the initial direction of the flow field. To the ramp problem, $\phi = 20^o$ (ramp inclination angle) and the freestream Mach number is 2.0, resulting from the β-diagram a value to β equals to 53.0º. Using a transfer in Figures 33 to 36, considering the xy plane, it is possible to

obtain the values of β to each scheme, as well the respective errors, shown in Tab. 3. As can be observed, the best scheme was the Yee (1987) symmetric Min1 one.

Table 3. Shock angle and respective percentage errors to the ramp problem (Laminar).

Algorithm	β(°)	Error (%)
Harten and Osher (1987) ENO	48.00	9.43
Harten and Osher (1987) TVD	54.20	2.26
Yee (1987) TVD Min1	53.00	0.00
Yee (1987) TVD Min2	52.80	0.38

4. CONCLUSIONS

In the present work, the Harten and Osher (1987) TVD/ENO and the Yee (1987) TVD symmetric schemes are implemented, on a finite volume context and using a structured spatial discretization, to solve the Euler and the laminar Navier-Stokes equations in the three-dimensional space. The Harten and Osher (1987) TVD/ENO schemes are flux difference splitting type, whereas the Yee (1987) TVD scheme is a symmetric one, which incorporates TVD properties due to the appropriated definition of a limited dissipation function. All schemes are second order accurate in space and their numerical implementation is based on the concept of Harten's modified flux function. All three schemes are implemented following an implicit formulation to solve the Euler equations. The flux difference splitting schemes employ approximate factorizations in Linearized Nonconservative Implicit LNI form, whereas the symmetric scheme employs approximate factorization in ADI form. The viscous simulations are treated with the explicit versions of the present algorithms, which employ a time splitting method. The schemes are accelerated to the steady state solution using a spatially variable time step, which has demonstrated effective gains in terms of convergence rate (Maciel, 2005 and 2008). The algorithms are applied to the solution of the physical problems of the transonic flow along a convergent-divergent nozzle and of the supersonic flow along a compression corner in the inviscid case, whereas the laminar case studies a particular ramp problem.

The results have demonstrated that the most accurate results are obtained with the Harten and Osher (1987) ENO and Yee (1987) TVD VL and Min1 schemes, obtaining more accurate values of the shock angle in the compression corner and ramp problems. The Yee (1987) TVD VL scheme also obtains the closest pressure distribution in the nozzle problem.

5. ACKNOWLEDGEMENTS

The author thanks the financial support conceded by CNPq under process number PDJ 150143/2008-7.

6. REFERENCES

Anderson Jr., J. D., 1984, "Fundamentals of Aerodynamics", McGraw-Hill, Inc., EUA, 563p.

Fox, R. W., and McDonald, A. T., 1988, "Introdução à Mecânica dos Fluidos", Ed. Guanabara Koogan, Rio de Janeiro, RJ, Brazil, 632p.

Harten, A., and Osher, S., 1987, "Uniformly High-Order Accurate Nonoscillatory Schemes I", SIAM Journal on Numerical Analysis, Vol. 24, No. 2, pp. 279-309.

Maciel, E. S. G., 2005, "Analysis of Convergence Acceleration Techniques Used in Unstructured Algorithms in the Solution of Aeronautical Problems – Part I", Proceedings of the XVIII International Congress of Mechanical Engineering (XVIII COBEM), Ouro Preto, MG, Brazil.

Maciel, E. S. G., 2008, "Analysis of Convergence Acceleration Techniques Used in Unstructured Algorithms in the Solution of Aerospace Problems – Part II", Proceedings of the XII Brazilian Congress of Thermal Engineering and Sciences (XII ENCIT), Belo Horizonte, MG, Brazil.

Maciel, E. S. G., 2009, "Explicit and Implicit TVD and ENO High Resolution Algorithms Applied to the Euler and Navier-Stokes Equations in Three-Dimensions – THEORY", Proceedings of the XX International Congress of Mechanical Engineering (XX COBEM), Gramado, RS, Brazil.

Mason, M. L., Putnam, L. E., and Re, R. J., 1980, "The Effect of Throat Contouring on Two-Dimensional Converging-Diverging Nozzles at Sonic Conditions", NASA Technical Paper 1704.

Yee, H. C., 1987, "Construction of Explicit and Implicit Symmetric TVD Schemes and Their Applications", Journal of Computational Physics, Vol. 68, pp. 151-179.

7. RESPONSIBILITY NOTICE

The author is the only responsible for the printed material included in this paper.